Patient iPSC-Derived Neurons for Disease Modeling of Frontotemporal Dementia with Mutation in *CHMP2B*

Yu Zhang,[1,*] Benjamin Schmid,[2] Nanett K. Nikolaisen,[1] Mikkel A. Rasmussen,[2] Blanca I. Aldana,[3] Mikkel Agger,[4] Kirstine Calloe,[5] Tina C. Stummann,[6] Hjalte M. Larsen,[1] Troels T. Nielsen,[7] Jinrong Huang,[8,9] Fengping Xu,[8,9] Xin Liu,[8,9] Lars Bolund,[10] Morten Meyer,[4] Lasse K. Bak,[3] Helle S. Waagepetersen,[3] Yonglun Luo,[10] Jørgen E. Nielsen,[7] The FReJA Consortium, Bjørn Holst,[2] Christian Clausen,[2] Poul Hyttel,[1] and Kristine K. Freude[1,*]

[1]Stem Cells and Embryology Group, Department of Veterinary Clinical and Animal Sciences, Faculty of Health and Medical Sciences, University of Copenhagen, 1870 Frederiksberg C, Denmark
[2]Bioneer A/S, 2970 Hørsholm, Denmark
[3]Neurometabolism Research Unit, Department of Drug Design and Pharmacology, Faculty of Health and Medical Sciences, University of Copenhagen, 2100 Copenhagen, Denmark
[4]Stem Cell and Developmental Neurobiology Group, Department of Neurobiology Research, University of Southern Denmark, 5000 Odense C, Denmark
[5]The Physiology Group, Department of Veterinary Clinical and Animal Sciences, Faculty of Health and Medical Sciences, University of Copenhagen, 1870 Frederiksberg C, Denmark
[6]H. Lundbeck A/S, 2500 Valby, Denmark
[7]Neurogenetics Clinic & Research Lab, Danish Dementia Research Centre, Department of Neurology, Rigshospitalet, University of Copenhagen, 2100 Copenhagen, Denmark
[8]BGI-Shenzhen, 518083 Shenzhen, China
[9]China National GeneBank-Shenzhen, BGI-Shenzhen, 518083 Shenzhen, China
[10]Danish Regenerative Engineering Alliance for Medicine (DREAM), Department of Biomedicine, Aarhus University, 8000 Aarhus C, Denmark
*Correspondence: yu.zhang@sund.ku.dk (Y.Z.), kkf@sund.ku.dk (K.K.F.)
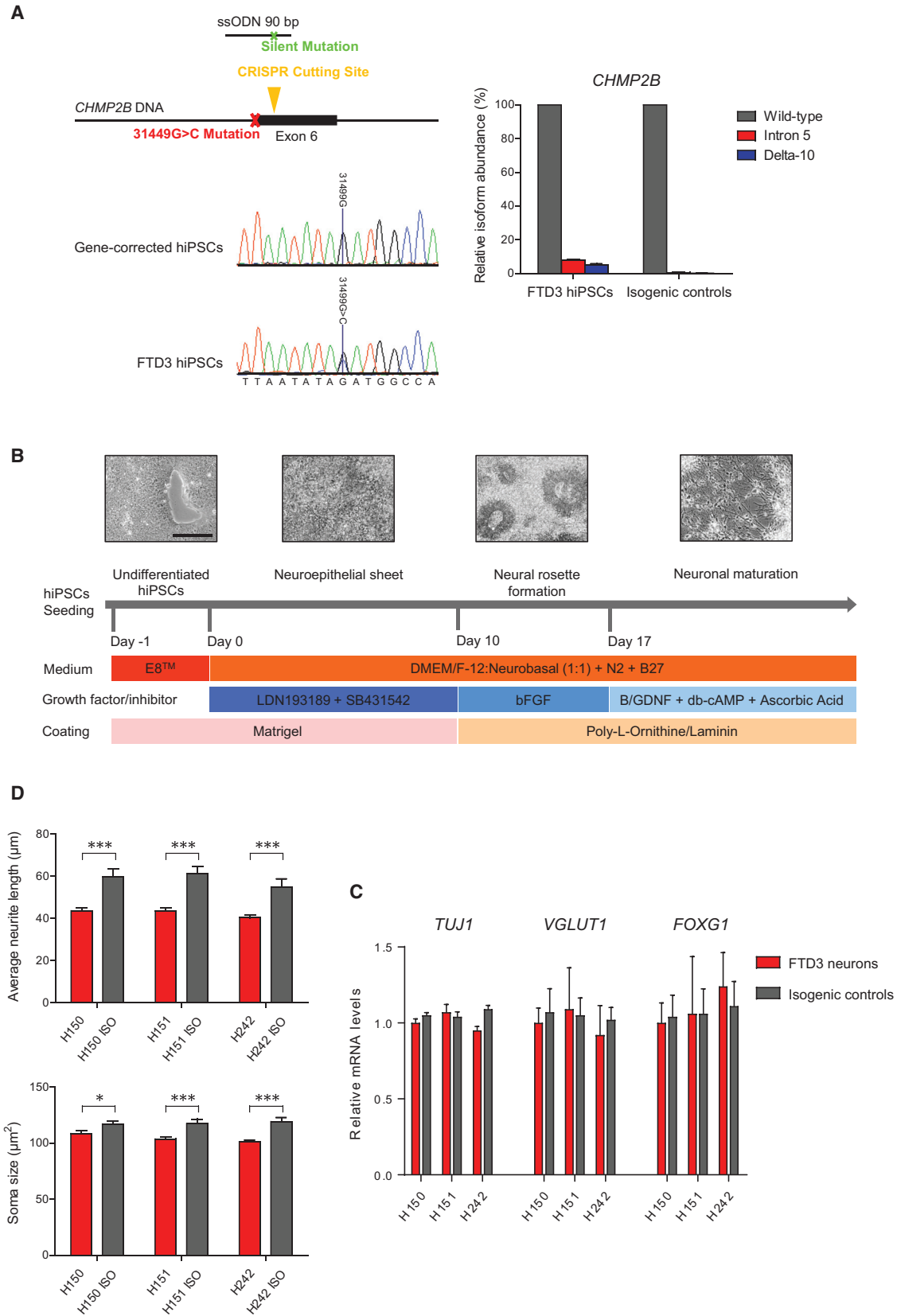http://dx.doi.org/10.1016/j.stemcr.2017.01.012

SUMMARY

The truncated mutant form of the charged multivesicular body protein 2B (CHMP2B) is causative for frontotemporal dementia linked to chromosome 3 (FTD3). CHMP2B is a constituent of the endosomal sorting complex required for transport (ESCRT) and, when mutated, disrupts endosome-to-lysosome trafficking and substrate degradation. To understand the underlying molecular pathology, FTD3 patient induced pluripotent stem cells (iPSCs) were differentiated into forebrain-type cortical neurons. FTD3 neurons exhibited abnormal endosomes, as previously shown in patients. Moreover, mitochondria of FTD3 neurons displayed defective cristae formation, accompanied by deficiencies in mitochondrial respiration and increased levels of reactive oxygen. In addition, we provide evidence for perturbed iron homeostasis, presenting an in vitro patient-specific model to study the effects of iron accumulation in neurodegenerative diseases. All phenotypes observed in FTD3 neurons were rescued in CRISPR/Cas9-edited isogenic controls. These findings illustrate the relevance of our patient-specific in vitro models and open up possibilities for drug target development.

INTRODUCTION

Frontotemporal dementia (FTD) is the second most common form of early-onset (<65 years) dementia, accounting for 5%–8% of total dementia cases. FTD is a neurodegenerative disorder with cognitive impairment affecting the frontal and/or temporal lobes of the brain associated with progressive brain atrophy (Rossor et al., 2010). FTD is clinically, neuropathologically, and genetically heterogeneous. One gene affected in familial cases is the charged multivesicular body protein 2B (*CHMP2B*) located on chromosome 3 (FTD3). Patients display global cortical and central brain atrophies, with no apparent amyloid plaque formation or conclusive hyperphosphorylated tau aggregates (Isaacs et al., 2011). Early behavioral changes include apathy, restlessness, disinhibition, and hyperorality. Late-stage behavioral changes include stereotype behavior, mutism, and dystonia (Isaacs et al., 2011). CHMP2B is a component of the endosomal sorting complex required for transport III

(ESCRT-III) complex, which facilitates recycling or degradation of cell surface receptors (Chassefeyre et al., 2015). As such, the FTD3-causing mutation of *CHMP2B* affects functionality of the endosome. Mouse and *Drosophila* FTD3 animal models have yielded valuable in vivo insights into the dysfunction of the endosomal lysosomal system and pathologic progression (Ahmad et al., 2009; Ghazi-Noori et al., 2012). However, transgene integration and species-specific differences may contribute to observed phenotypes in such models. Hence, there is an emerging need for human FTD3 models. In addition, studying how *CHMP2B*, as a rare mutation, contributes to neurodegenerative disorders has not yet attracted broader attention. Consequently, a *CHMP2B* mutant cellular model could provide further insights into common underlying dysfunction of biological pathways, disrupted or disturbed in neurodegenerative diseases and thereby linking different forms of neurodegeneration.

The availability of viable neurons from patient brains, at least in part, limits the investigation of the mechanism of

CrossMark

A

ssODN 90 bp

Silent Mutation

CRISPR Cutting Site

CHMP2B DNA

31449G>C Mutation   Exon 6

Gene-corrected hiPSCs

31499G

FTD3 hiPSCs

31499G>C

T T A A T A T A G A T G G C C A

CHMP2B

- Wild-type
- Intron 5
- Delta-10

Relative isoform abundance (%)

FTD3 hiPSCs   Isogenic controls

B

hiPSCs Seeding

| | Undifferentiated hiPSCs | Neuroepithelial sheet | Neural rosette formation | Neuronal maturation |

Day -1   Day 0   Day 10   Day 17

Medium: E8™ | DMEM/F-12:Neurobasal (1:1) + N2 + B27

Growth factor/inhibitor: LDN193189 + SB431542 | bFGF | B/GDNF + db-cAMP + Ascorbic Acid

Coating: Matrigel | Poly-L-Ornithine/Laminin

D

Average neurite length (μm)

*** *** ***

H150 H150 ISO H151 H151 ISO H242 H242 ISO

Soma size (μm²)

* *** ***

H150 H150 ISO H151 H151 ISO H242 H242 ISO

C

Relative mRNA levels

TUJ1   VGLUT1   FOXG1

- FTD3 neurons
- Isogenic controls

H150 H151 H242   H150 H151 H242   H150 H151 H242

neurodegenerative pathogenesis. In this context, human-induced pluripotent stem cells (iPSCs) provide invaluable access to study the disease progression in neurons derived from patient iPSCs and facilitate the development of new therapies (Ehrlich et al., 2015; Rasmussen et al., 2014). Meanwhile, recent advances of state-of-the-art genome engineering technique CRISPR/Cas9 (Ran et al., 2013) have had a tremendous impact allowing for gene correction in patients who are carriers of disease-causing single-point mutations. Such genetically edited iPSCs are ideal isogenic controls for the patient-derived iPSCs, allowing to precisely dissect the significance of the disease-causing mutation while maintaining the patient's own genetic background.

To study the cellular and molecular events of FTD3, we derived a disease model using human iPSCs from patients carrying the 31449G > C mutation in *CHMP2B* and isogenic controls generated via the CRISPR/Cas9 system with subsequent in vitro neuronal differentiation. Our model not only confirmed partly prior-observed pathologies in animal models such as endosome dysregulation (Ghazi-Noori et al., 2012), but also revealed additional disease-relevant phenotypes in FTD3 by way of abnormal mitochondrial ultrastructure and function. Moreover, RNA sequencing (RNA-seq) uncovered that the *CHMP2B* mutation manifests in dysregulated expression of key genes associated with Parkinson's disease (PD) and Alzheimer's disease (AD) and indicated that perturbed iron homeostasis is one of the underlying disease mechanisms.

RESULTS

Generation of FTD3 iPSCs and Genetically Corrected Isogenic Controls

Skin fibroblasts from two symptomatic FTD3 patients (H150 and H151) and one presymptomatic FTD3 patient (H242) were reprogrammed using non-integrative episomal plasmids. All of these individuals are from the same family, and one independent healthy control from an unrelated family was also included. Individual FTD3 iPSC lines were assessed for pluripotency features via qPCR (Figure S1A)

and immunocytochemistry (ICC) (Figure S1B). Assessment of pluripotency potential was confirmed via embryoid body formation and subsequent spontaneous differentiation (Figure S1C). The FTD3-causing mutation 31449G > C (located at the splice acceptor site in *CHMP2B*, at the border of intron 5 and exon 6) was repaired in the FTD3 iPSC lines using the CRISPR/Cas9 system (Figure 1A). The presence of altered *CHMP2B* mRNA, as formerly shown in Urwin et al. (2010) was confirmed via qPCR and showed expression of the intron 5 and delta-10 isoforms only in the patient iPSC. These abnormal transcripts, generated via the CHMP2B mutation affecting the slice acceptor site, are completely absent in the isogenic controls (Figure 1A). All iPSC and genetically corrected isogenic lines were determined to be karyotypically normal (Figure S1D).

Differentiation of FTD3 iPSCs to Forebrain Cortical Neurons

We employed a modified dual SMAD protocol (Figure 1B) to generate forebrain-specific cortical neurons. Flow cytometry analyses demonstrated the neural progenitor cell (NPC) cultures to be comparable with respect to NESTIN and SOX1 expression (Figure S2A). All NPCs expressed the forebrain markers PAX6 and OTX2 (Figure S2B). ICC revealed the majority of the matured neurons to be glutamatergic (immunopositive for VGlut1 [Figure S2C] and co-positive for MAP2, TAU, and TUJ1 [Figure S2C]). Approximately 10% of neurons were GABAergic (Figure S2C), while approximately 5% were GFAP-positive astrocytes, with a minor population (2%–3%) comprising tyrosine hydroxylase-positive dopaminergic neurons (Figure S2C). Since quantification via ICC is challenging we performed qPCR for *TUJ1*, *VGlut1*, and FOXG1 in order to estimate the comparability in regard to the neural cell composition of the investigated FTD3 iPSC- and isogenic iPSC-derived neurons. All lines showed comparable amounts of expression with no significant differences, which is also indicative that the mutation in *CHMP2B* does not affect the differentiation potential toward neurons (Figure 1C). Neurons exhibited spiking activity and action potentials, which occurred both spontaneously
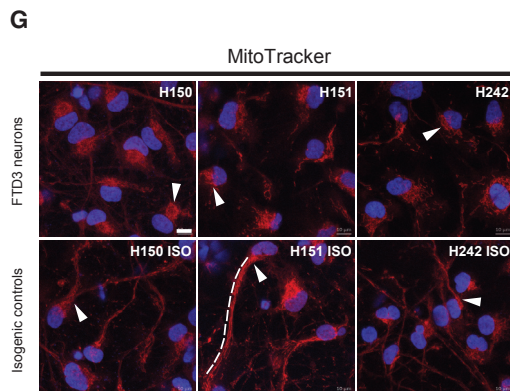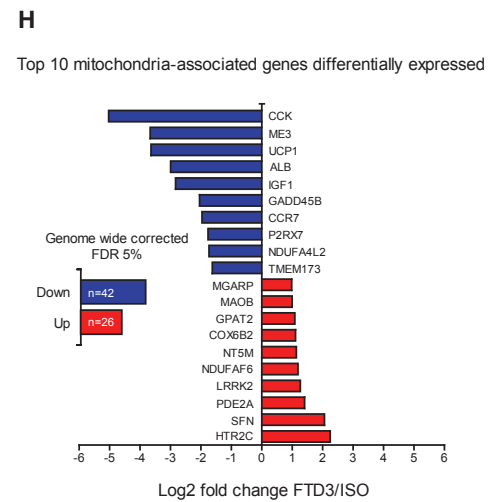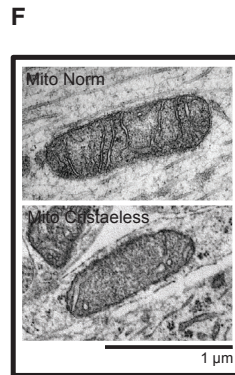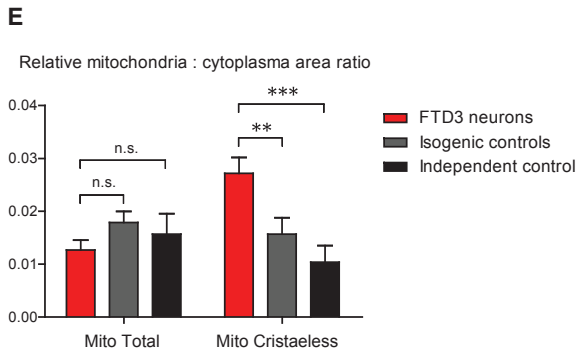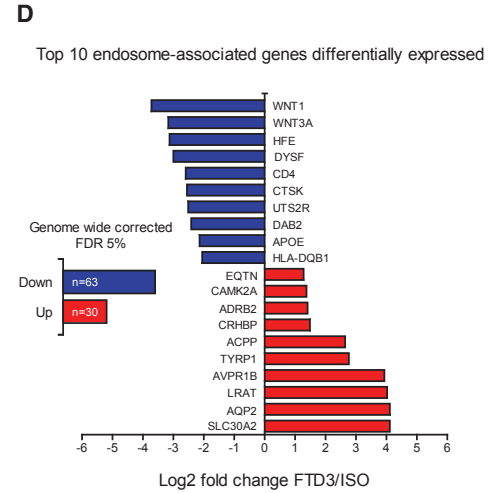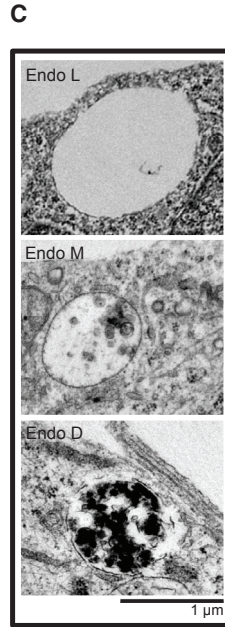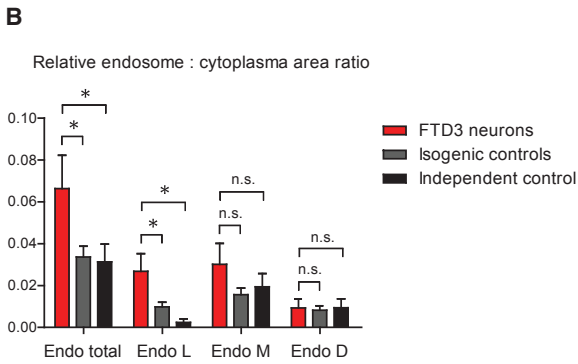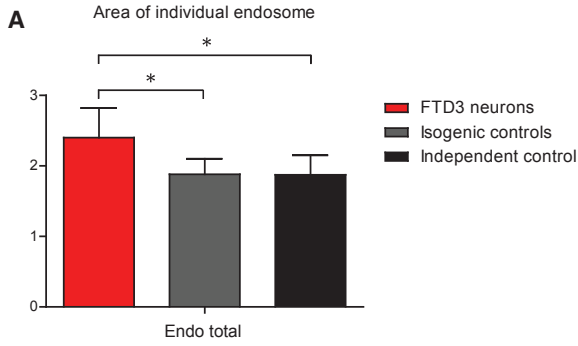

Figure 1. Gene Correction of FTD3 iPSCs, In Vitro Neuronal Differentiation, and Morphometric Analyses

(A) CRISPR/Cas9-mediated gene correction of *CHMP2B* 31449G > C, ssODN with silent mutation (*Sac*II), sequencing results, and quantification of *CHMP2B* mutant and wild-type mRNA transcripts. The expression values were calculated as relative amount of mRNA versus expression values of wild-type which was set to 100%.

(B) Schematic of neuronal differentiation protocol (see Experimental Procedures for details). Scale bar, 200 μm for all. BFGF, basic fibroblast growth factor; GDNF, glial cell line-derived neurotrophic factor; cAMP, cyclic AMP.

(C) Quantification of *TUJ1*, *VGlut1*, and FOXG1 mRNA expression levels in FTD3 neurons (H150, H151, H242) and isogenic controls (H150 ISO, H151 ISO, H242 ISO). n = 3 with three replicates in each experiment, no significant differences were found among the different lines.

(D) Morphometric analyses in FTD3 neurons and isogenic controls: Average neurite length and soma size. n = 3 with three replicates in each experiment, significant differences are indicated by *p < 0.05 and ***p < 0.001.

A Area of individual endosome

FTD3 neurons
Isogenic controls
Independent control

Endo total

B Relative endosome : cytoplasma area ratio

FTD3 neurons
Isogenic controls
Independent control

Endo total Endo L Endo M Endo D

C

Endo L

Endo M

Endo D

1 μm

D Top 10 endosome-associated genes differentially expressed

WNT1
WNT3A
HFE
DYSF
CD4
CTSK
UTS2R
DAB2
APOE
HLA-DQB1
EQTN
CAMK2A
ADRB2
CRHBP
ACPP
TYRP1
AVPR1B
LRAT
AQP2
SLC30A2

Genome wide corrected FDR 5%

Down n=63
Up n=30

Log2 fold change FTD3/ISO

E Relative mitochondria : cytoplasma area ratio

FTD3 neurons
Isogenic controls
Independent control

Mito Total Mito Cristaeless

n.s. n.s. ** ***

F

Mito Norm

Mito Cristaeless

1 μm

G MitoTracker

FTD3 neurons

H150 H151 H242

Isogenic controls

H150 ISO H151 ISO H242 ISO

H Top 10 mitochondria-associated genes differentially expressed

CCK
ME3
UCP1
ALB
IGF1
GADD45B
CCR7
P2RX7
NDUFA4L2
TMEM173
MGARP
MAOB
GPAT2
COX6B2
NT5M
NDUFAF6
LRRK2
PDE2A
SFN
HTR2C

Genome wide corrected FDR 5%

Down n=42
Up n=26

Log2 fold change FTD3/ISO

(legend on next page)

and under current-clamp conditions (Figures S3B–S3D). Measurement of intracellular calcium levels also demonstrated that cultures exhibited neuronal functionality. The neurons were responsive to the neurotransmitters glutamate/glycine, GABA, and, to a lesser extent, acetylcholine (Figure S3A), and depolarization of the plasma membrane by addition of potassium resulted in a small increase in intracellular calcium (Figure S3A). Serotonin and dopamine did not induce a change in intracellular calcium levels. All lines showed similar responses.

FTD3 Neurons Display Aberrant Endosomes

Via transmission electron microscopy, we observed similarly enlarged endosome (assessed as endosome-occupied relative neuronal area, see the Supplemental Experimental Procedures) in our FTD3 neurons, as previously demonstrated in patients (Urwin et al., 2010) (Figure 2A). Such enlarged endosomes were absent from the isogenic controls, indicating a rescue of the phenotype by CRISPR/Cas9-mediated gene correction and is consistent with previous knockdown experiments (Nielsen et al., 2012). Specifically, the electron-lucent and, thus, vacant endosomes were significantly more abundant in the FTD3 neurons (Figures 2B and 2C), indicative of an effect on early-stage endosomes.

FTD3 Neurons Display Abnormal Mitochondria

Given that mitochondrial defects are commonly observed in neurodegenerative diseases, we assessed whether such a phenotype is evident in FTD3 neurons. While we noted no apparent difference in size of mitochondria between FTD3 neurons and their isogenic controls, we did observe a significant increase in abnormal mitochondria with severe impairment of cristae formation in FTD3 neurons (Figures 2E and 2F). Strikingly, the distribution of mitochondria within neurons was also perturbed in FTD3 neurons: MitoTracker analyses revealed mitochondria in FTD3 neurons to preferentially localize to the perinuclear region, while isogenic controls exhibited a homogeneous distribution throughout axons and dendrites (Figure 2G). Consistent with previous studies correlating a lack of axonal mitochondria with axonal degradation (Rawson et al., 2014), we also observed disorganized microtubule organization in FTD3 neurons (Figure S4A). These findings were substantiated by the fact that the average neurite length and soma size were significantly reduced in FTD3 neurons versus isogenic controls (Figure 1D).

FTD3 Neurons Display Impaired Mitochondria Function and Increased Oxidative Stress

Prompted by our observations of aberrant mitochondrial morphology, we sought to test the functionality of such FTD3 mitochondria by assessing their basal respiration rate, ATP-linked respiration, proton leak, and reserve capacity. Our analyses uncovered a reduced basal respiration rate in FTD3 neurons as well as a reduced maximal capacity (Figure 3E). Consistent with mitochondrial dysfunction manifesting in oxidative stress, we observed up to 20% occurrence of oxidative stress in FTD3 neurons compared with only 7% in isogenic controls (Figure 3A). Thus, FTD3 neurons are exposed to higher levels of oxidative stress, and targeted gene editing can reverse the disease phenotype. Subsequently, we investigated whether the increased oxidative stress impacts cell viability, but we detected no evidence for increased apoptosis in FTD3 neurons (Figure 3B).

Global Gene Expression Analyses Confirm Defects in the Endosome, Mitochondrial Dysfunction, and Increased Oxidative Stress

To obtain an overview of gene expression changes in CHMP2B-dependent neurodegeneration, we performed

Figure 2. FTD3 Neurons Exhibit Aberrant Endosome and Mitochondria
(A and B) Stereology and ultrastructure of endosome in FTD3 neurons (red bar), isogenic controls (gray bar), and an independent healthy control (black bar): (A) shows total size of endosome; (B) shows the ratio of endosome to cytoplasm and further subdivision by appearance into electron-lucent (Endo L), medium electron-dense (Endo M), and electron-dense (Endo D); n = 3 with three replicates in each experiment, significant differences are indicated by *p < 0.05. n.s., not significant.
(C) Transmission electron microscopy (TEM) images of Endo L, Endo M, and Endo (D) Scale bar, 1 μm for all.
(D) Total number of endosome-associated genes and the top ten differentially expressed genes (on the basis of fold-change) within a false discovery rate (FDR) of 5%.
(E) Stereology and ultrastructure of mitochondria in FTD3 neurons (red bar), isogenic controls (gray bar), and an independent healthy control (black bar): relative size of mitochondria compared with cytoplasmic area of all mitochondria (Mito total) and cristaeless mitochondria; n = 3 with three replicates in each experiment, significant differences are indicated by **p < 0.01, and ***p < 0.001.
(F) TEM images of normal and cristaeless mitochondria. Scale bar, 1 μm for both.
(G) Images of neurons dyed with the mitochondrial probe MitoTracker (red) counterstained with DAPI (blue). Arrowheads indicate dyed mitochondria and the dashed line shows a representative distribution of mitochondria in an isogenic control neuron. Scale bar, 10 μm for all.
(H) Total number of mitochondria-associated genes and top ten differentially expressed genes (on the basis of fold-change) within an FDR of 5%.
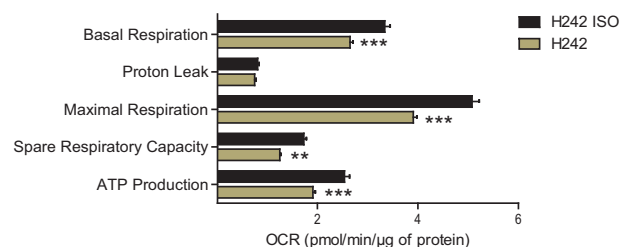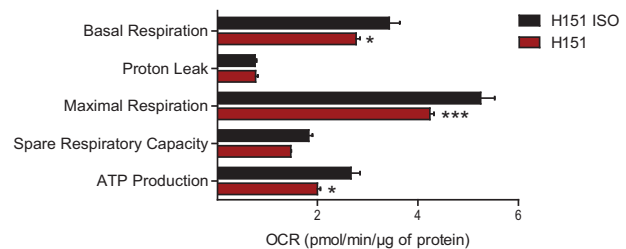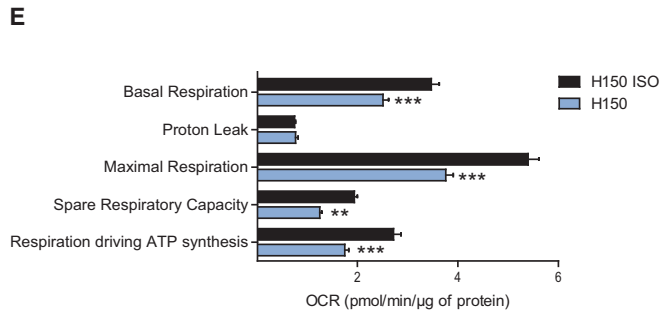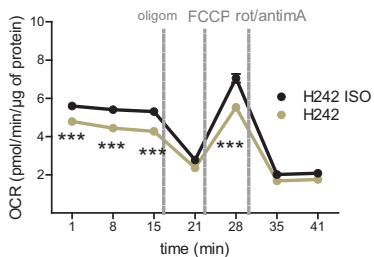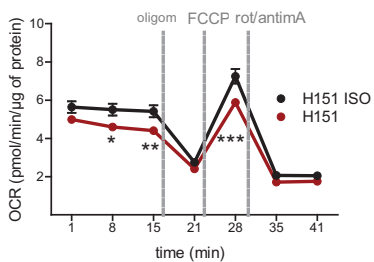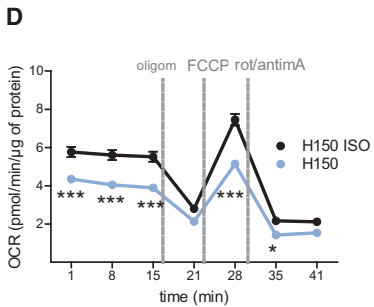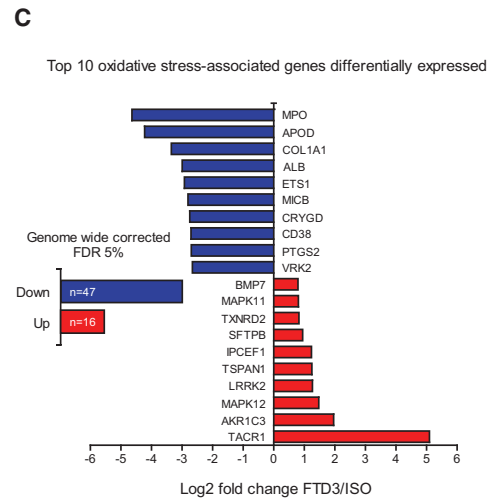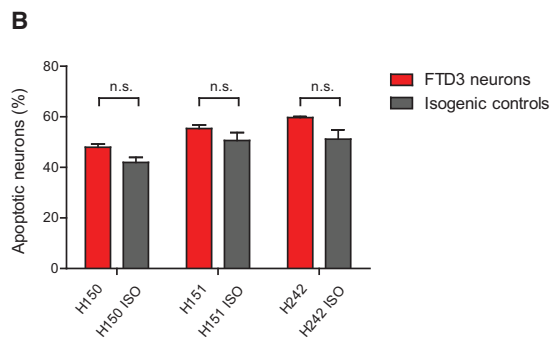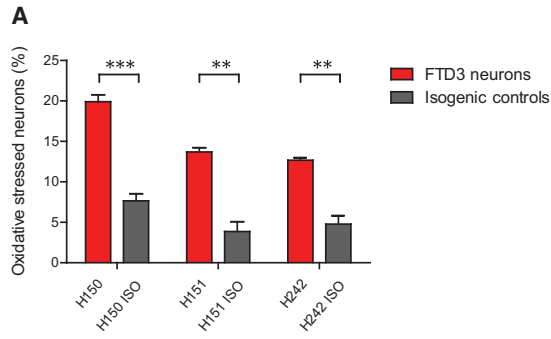
(legend on next page)

RNA-seq analyses, which revealed 3,205 differentially expressed genes in FTD3 neurons compared with their isogenic controls. Heatmap analyses showed that neurons derived from iPSCs of all three FTD3 individuals clustered together, while isogenic controls clustered together with the independent healthy individual (Figure 4A), suggesting that the isogenic control lines reverted to a healthy control gene expression profile after repair of the *CHMP2B* mutation. To identify which cellular components are primarily affected in FTD3 neurons, we performed gene ontology (GO) term analysis. We found enrichment of the GO term for postsynaptic membrane, synaptic membrane, neuron projection, and synaptic vesicle membrane (Figure 4C), and depletion of early endosome membrane, lysosomal lumen, and endocytic vesicle membrane (Figure 4D).

With the aim to identify additional genes associated with the main phenotypes observed in FTD3 neurons, we extracted the top ten differentially regulated genes functionally linked to neurodegeneration and associated with endosomes (Figure 2D), mitochondria (Figure 2H), and oxidative stress (Figure 3C). Strikingly, *APOE* ranked among the ten most downregulated endosome-associated genes (Figure 2D). APOE4, an isoform of APOE, is a well-known risk factor for sporadic AD (sAD) (Corder et al., 1993) and, consistent with a putative role in FTD3 pathophysiology, some sAD patients present with enlarged early endosomes (Cataldo et al., 2000).

Most interestingly, we observed an upregulation of leucine-rich repeat kinase 2 (*LRRK2*) among the mitochondria-related genes (Figure 2H). *LRRK2* is one of the five genes mutated in familial forms of PD. Previous studies reported mitochondrial fragmentation due to increased expression of *LRRK* (Wang et al., 2012), pointing to an association between upregulated *LRRK2* expression and cristae dysgenesis in FTD3 neurons. *LRRK2* was also detected in the oxidative stress group (Figure 3C) and is upregulated in some cases of sporadic PD (Cho et al., 2013) accompanied by elevated levels of oxidative stress (Nguyen et al., 2011). *MPO* and *APOD*, both implicated in AD (Figure 3C) (Maki et al., 2009; Martinez et al., 2012), were strongly downregulated in FTD3 neurons.

Imbalance of Iron Homeostasis Represents a Unifying Factor Linking Endosome, Mitochondrial Dysfunction, and Oxidative Stress

Via our in silico analyses, we identified mis-expression of genes encoding proteins or receptors known to be involved in iron homeostasis. Among these were *TRPC6* (12-fold upregulated), *HFE* (8-fold downregulated), and *ABCG2*, *HP*, and *CP* (all 2-fold downregulated) (Figure 4B). A potential imbalance of iron homeostasis might plausibly induce intracellular ferrous iron (Fe^{2+}) accumulation, damaging mitochondria and inducing stress, to be further exacerbated by the defects in the endosome compartment contributing to increased amounts of trapped Fe^{3+} within endosomes (Figure 4E). Supporting this hypothesis, cytoplasmic Fe^{2+} levels are significantly increased in FTD3 neurons versus isogenic control neurons (Figure 4F). This increase in intracellular iron was consistent in several independent neural differentiation experiments, and the increased expression in TRCP6 was also confirmed via western blot analysis (Figure 4B), further substantiating our hypothesis for impaired iron homeostasis triggered by altered expression and protein amounts of key regulators.

Taken together we have shown that FTD3 neurons have enlarged early endosomes, display mitochondria dysfunction and perturbed iron homeostasis, with subsequent increase in oxidative stress.

DISCUSSION

The biological function of CHMP2B has primarily been investigated in animal models, with the attendant caveat that observed phenotypes are potentially species specific or contributed to by transgene integration. Here, to preclude such issues, we developed an FTD3 patient-derived disease model by way of iPSCs generation, genome editing, and in vitro neuronal differentiation techniques.

We identified enlargements of particularly the early endosome population in FTD3 neurons, indicating that perturbed endo-lysosomal fusion and degradation of substrates is key to the underlying FTD3 pathophysiology. Cellular

**Figure 3. Impaired Mitochondrial Function and Oxidative Stress in FTD3 Neurons**
(A) CellROX green and SYTOX red flow cytometry assay of live oxidative stressed neurons. n = 3 with three replicates in each experiment, significant differences are indicated by **p < 0.01 and ***p < 0.001.
(B) CellEvent Caspase-3/7 green and SYTOX red flow cytometry assay of apoptotic neurons.
(C) Total number of oxidative stress-associated genes and the top ten differentially expressed genes (on the basis of fold-change) within an FDR of 5%. n.s., not significant.
(D and E) Mitochondrial function profile of FTD3 neurons (H150, H151 and H242) and isogenic controls (H150 ISO, H151 ISO, H242 ISO).
(D) oxygen consumption rate (OCR) was measured before (basal) and after the addition of oligomycin (oligom), carbonyl cyanide-4-(trifluoromethoxy)phenylhydrazone (FCCP), and a mixture of rotenone (rot) and antimycin A (antimA), respectively; (E) mitochondrial respiration parameters were calculated based on the OCR measurements shown in (D) as described in the Supplemental Experimental Procedures. n = 3 with three replicates in each experiment, significant differences are indicated by *p < 0.05, **p < 0.01, and ***p < 0.001.

A

B
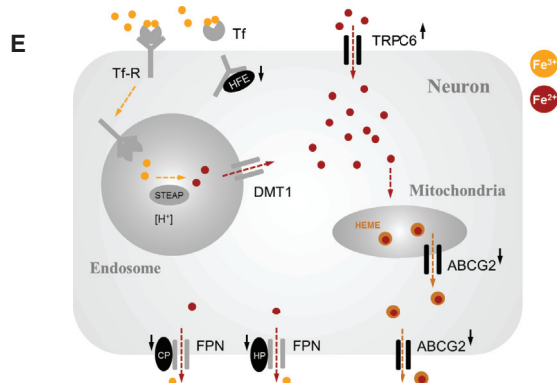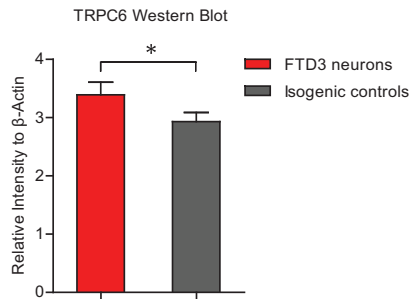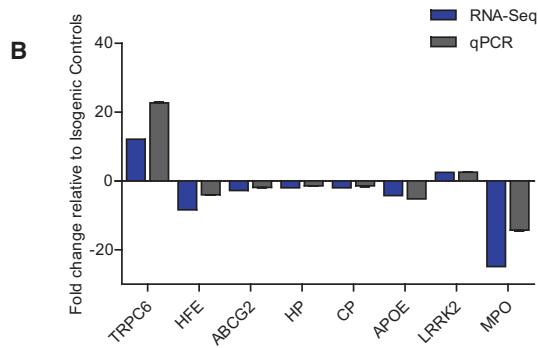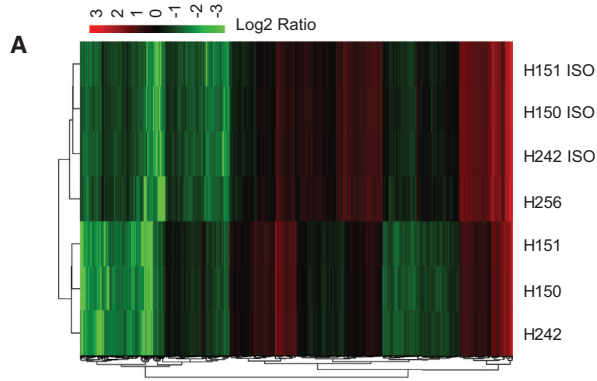
C

Up-regulated GO terms (cellular component) enrichment

D

Down-regulated GO terms (cellular component) enrichment

E

F
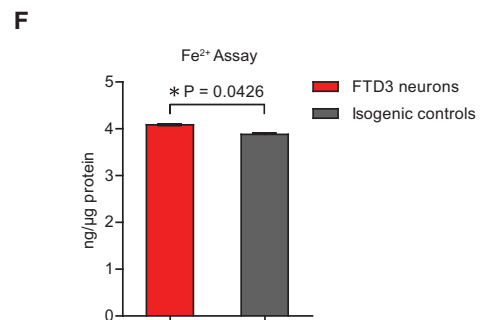
(legend on next page)

components, including mitochondria, are degraded in the endosome; in amyotrophic lateral sclerosis, a progressive lysosomal deficit is causative for impaired degradation of damaged mitochondria in motor neurons (Xie et al., 2015). Defective recycling of large organelles, such as mitochondria, is the earliest detectable impairment in a chain of events initiated by defective recycling (Cannizzo et al., 2012), which clearly links endosome and mitochondrial dysfunction.

FTD3 neurons displayed abnormal mitochondrial localization and cristae formation, manifesting in impaired functionality typical for neurodegenerative diseases. Defective mitochondria show impaired ATP generation and release of deleterious chemicals such as reactive oxygen species (ROS), potentially inducing cell death. We contend that increased ROS release contributes to increased organelle damage, which cannot be appropriately ameliorated through degradation owing to the observed endosome defects, resulting in a self-perpetuating cycle of cellular damage.

Strikingly, in FTD3 neurons we identified a robust, significant upregulation of *LRRK2* encoding the dardarin protein. One function of dardarin is the modulation of intracellular trafficking via recruitment of RAB7 (Greggio et al., 2006). Mutant CHMP2B impairs the recruitment of RAB7, crucial for endosome-lysosome fusion (Urwin et al., 2010). This relationship between CHMP2B, RAB7, and dardarin is supported by studies showing that dardarin negatively regulates RAB7-dependent localization of the lysosome (Dodson et al., 2012). Therefore, upregulation of *LRRK2* as a consequence of *CHMP2B* mutation might contribute to deficient endo-lysosomal trafficking and fusion. Dardarin also plays a role in mitochondrial functionality and positioning, since induced expression of *wild-type LRRK2* induces mitochondrial fragmentation via increased fission and upregulation of *DLP1*, which is critical for correct mitochondrial distribution (Wang et al., 2012).

Furthermore, our analysis revealed *APOE* to be significantly downregulated in FTD3 neural cells. The cells analyzed via RNA-seq are a mixed population of neurons and glial cells, with an up to 90% enrichment of VGlut1+

neurons. Due to this mixed population of cells we were still able to detect *APOE* via RNA-seq, even though it is mainly expressed in astrocytes. APOE is a major cholesterol carrier in neurons that supports lipid transport and brain injury repair, and there is a key requirement for APOE in facilitating the clearance of soluble amyloid beta (Abeta) (Jiang et al., 2008). Furthermore, APOE suppresses microglia activation (Laskowitz et al., 2001), and reduced APOE levels might potentially trigger inflammatory events. Together, this suggests that downregulation of APOE in FTD3 neurons might be a contributing factor in the microglia activation seen in postmortem FTD3 brains. Interestingly, we observed another phenotype restricted to glial cells. It has previously been reported for FTD3 mouse models and patient brains that these display p62 inclusions, which are indicative for impaired autophagy, oxidative stress, and neurotoxicity (Ghazi-Noori et al., 2012; Holm et al., 2007). We identified these p62 inclusions only in the S100β+ glial cell population and not in our TUJ1+ neurons (Figure S4B). Both the APOE and the p62 phenotypes clearly show that, even though several disease features can be replicated in our FTD3 neurons, other neural cell types need to be investigated in the future to understand the full complexity and pathophysiology of the disease.

Based on the differentially expressed key components and increase of intracellular iron in FTD3 neurons, we present an additional pathological feature of FTD3, which is associated with an imbalance in iron homeostasis (Figure 4E). Iron uptake principally proceeds through iron bound to transferrin mediated via the transferrin receptor or via direct uptake of Fe^{2+} facilitated by a variety of receptors including TRPC6 (Mwanjewe and Grover, 2004). We propose that upregulation of TRPC6 manifests in increased uptake of Fe^{2+}, while downregulation of HFE (which competes with Tf), results in uptake of more ferric iron which can further be reduced into Fe^{2+}. In contrast, export of heme-bound iron via ABCG2 or unbound Fe^{2+} through FPN can be reduced. Concordant with this model, we confirmed in several individual differentiation experiments a small but significant increase of intracellular iron within 5 weeks of neuronal differentiation in FTD3 neurons. Excessive amounts of intracellular Fe^{2+} are toxic to

Figure 4. Transcriptional Analysis of FTD3 Neurons Versus Isogenic Controls and Quantification of Intracellular Fe^{2+} Content
(A) Heatmap and hierarchical clustering analysis of gene expression profile of FTD3 neurons (H150, H151, H242) and isogenic controls (H150 ISO, H151 ISO, H242 ISO) as well as one independent healthy control (H256).
(B) qPCR validation of genes of interest from RNA-seq results and western blot relative quantification of TRPC6 protein expression.
(C and D) GO term enrichment analysis of differentially expressed genes via ClueGO v1.4 software. Functionally grouped network with terms as nodes linked based on their kappa score level (≥ 0.5), where only the label of the most significant term per group is shown. The node size represents the term enrichment significance. Functionally related groups partially overlap.
(E) Diagram of key dysregulated genes involved in intracellular iron homeostasis.
(F) Fe^{2+} assay and concentration normalized to total cellular protein. n = 3 with three replicates in each experiment, significant differences are indicated by *p < 0.05.

cells and trigger the production of ROS. Moreover, Fe^{2+} and hydrogen peroxide engage in the so-called Fenton reaction, producing ferric iron and highly reactive hydroxide, which damages DNA, proteins, and lipids in the cell (Altamura and Muckenthaler, 2009).

FTD3 neurons present with enlarged early endosomes, increased cristaeless mitochondria, intracellular iron accumulation, and oxidative stress. All of these phenotypes were rescued via genetic correction of the CHMP2B mutation.

We propose that in FTD3 neurons two events occur in parallel: (1) mutant CHMP2B causes an imbalance in iron homeostasis triggering mitochondrial impairment, which consequently triggers ROS and neuronal damage, and (2) mutant CHMP2B-dependent enlargement of endosomes, which causes defects of the endo-lysosomal degradation and recycling pathway, including recycling of receptors for iron uptake, results in accumulation of defective mitochondria, imbalanced iron homeostasis, ROS, and neuronal damage. Future studies will determine the exact role of mutant CHMP2B on a molecular level within these cellular events.

In conclusion, our findings indicate a possibility of targeting iron imbalances therapeutically in efforts to intervene in this cycle of damage to attempt treatment of FTD3. Furthermore, the CHMP2B-dependent human iPSC-derived neurons can be added to the list of in vitro cellular model systems that serve as a tool to study not only common mechanisms of pathogenesis, such as mitochondrial defects and oxidative stress, but also the effects of iron accumulation in neurodegenerative diseases.

EXPERIMENTAL PROCEDURES

Cell Culture, iPSC Generation, and Neuronal Differentiation

iPSCs were generated via episomal reprogramming (Addgene, 27077, 27078, 27080) from human dermal fibroblasts obtained from skin biopsies. Neuronal differentiation followed a modified dual SMAD protocol.

Genome Editing

Generation of isogenic controls from the three FTD3 iPSC lines was achieved via the CRISPR/Cas9 system (Addgene, 62988) using single-strand donor oligonucleotides as a template.

Transmission Electron Microscopy

Cells were seeded on 13 mm Thermanox plastic coverslips (Nunc, 174950) coated with poly-O-Lysine/laminin. Ultra-thin (50–70 nm) sections were prepared, contrasted with 2% uranyl acetate (PolyScience, 21447) and lead citrate, and examined using a Philips CM100 transmission electron microscope equipped with a Morada camera.

RNA-Seq Analysis

For deep RNA-seq, libraries of FTD3 neurons, isogenic controls, and an independent healthy control were prepared and sequenced on a HiSeq 2000 Sequencing System (Illumina) following the manufacturer's protocol.

Statistical Analysis

Data are presented as mean ± SE. n is the number of independent differentiations of NPCs (from the cryobank) to neurons. Significance of data was evaluated by Student's t test or two-way ANOVA with Bonferroni post hoc test. Unless noted otherwise, $p < 0.05$ was considered statistically significant.

For further details on Experimental Procedures, see the Supplemental Information.

ACCESSION NUMBERS

The RNA-seq data described in this study have been deposited in the NCBI GEO database under accession number GEO: GSE92340.

SUPPLEMENTAL INFORMATION

Supplemental Information includes Supplemental Experimental Procedures, four figures, and one table and can be found with this article online at http://dx.doi.org/10.1016/j.stemcr.2017.01.012.

AUTHOR CONTRIBUTIONS

ACKNOWLEDGMENTS

REFERENCES

Ahmad, S.T., Sweeney, S.T., Lee, J.A., Sweeney, N.T., and Gao, F.B. (2009). Genetic screen identifies serpin5 as a regulator of the toll

pathway and CHMP2B toxicity associated with frontotemporal dementia. Proc. Natl. Acad. Sci. USA *106*, 12168–12173.

Altamura, S., and Muckenthaler, M.U. (2009). Iron toxicity in diseases of aging: Alzheimer's disease, Parkinson's disease and atherosclerosis. J. Alzheimers Dis. *16*, 879–895.

Cannizzo, E.S., Clement, C.C., Morozova, K., Valdor, R., Kaushik, S., Almeida, L.N., Follo, C., Sahu, R., Cuervo, A.M., Macian, F., et al. (2012). Age-related oxidative stress compromises endosomal proteostasis. Cell Rep. *2*, 136–149.

Cataldo, A.M., Peterhoff, C.M., Troncoso, J.C., Gomez-Isla, T., Hyman, B.T., and Nixon, R.A. (2000). Endocytic pathway abnormalities precede amyloid beta deposition in sporadic Alzheimer's disease and Down syndrome: differential effects of APOE genotype and presenilin mutations. Am. J. Pathol. *157*, 277–286.

Chassefeyre, R., Martinez-Hernandez, J., Bertaso, F., Bouquier, N., Blot, B., Laporte, M., Fraboulet, S., Coute, Y., Devoy, A., Isaacs, A.M., et al. (2015). Regulation of postsynaptic function by the dementia-related ESCRT-III subunit CHMP2B. J. Neurosci. *35*, 3155–3173.

Cho, H.J., Liu, G., Jin, S.M., Parisiadou, L., Xie, C., Yu, J., Sun, L., Ma, B., Ding, J., Vancraenenbroeck, R., et al. (2013). MicroRNA-205 regulates the expression of Parkinson's disease-related leucine-rich repeat kinase 2 protein. Hum. Mol. Genet. *22*, 608–620.

Corder, E.H., Saunders, A.M., Strittmatter, W.J., Schmechel, D.E., Gaskell, P.C., Small, G.W., Roses, A.D., Haines, J.L., and Pericak-Vance, M.A. (1993). Gene dose of apolipoprotein E type 4 allele and the risk of Alzheimer's disease in late onset families. Science *261*, 921–923.

Dodson, M.W., Zhang, T., Jiang, C., Chen, S., and Guo, M. (2012). Roles of the *Drosophila* LRRK2 homolog in Rab7-dependent lysosomal positioning. Hum. Mol. Genet. *21*, 1350–1363.

Ehrlich, M., Hallmann, A.L., Reinhardt, P., Arauzo-Bravo, M.J., Korr, S., Ropke, A., Psathaki, O.E., Ehling, P., Meuth, S.G., Oblak, A.L., et al. (2015). Distinct neurodegenerative changes in an induced pluripotent stem cell model of frontotemporal dementia linked to mutant TAU protein. Stem Cell Rep. *5*, 83–96.

Ghazi-Noori, S., Froud, K.E., Mizielinska, S., Powell, C., Smidak, M., de Marco, M.F., O'Malley, C., Farmer, M., Parkinson, N., Fisher, E.M.C., et al. (2012). Progressive neuronal inclusion formation and axonal degeneration in CHMP2B mutant transgenic mice. Brain *135*, 819–832.

Greggio, E., Jain, S., Kingsbury, A., Bandopadhyay, R., Lewis, P., Kaganovich, A., van der Brug, M.P., Beilina, A., Blackinton, J., Thomas, K.J., et al. (2006). Kinase activity is required for the toxic effects of mutant LRRK2/dardarin. Neurobiol. Dis. *23*, 329–341.

Holm, I.E., Englund, E., Mackenzie, I.R., Johannsen, P., and Isaacs, A.M. (2007). A reassessment of the neuropathology of frontotemporal dementia linked to chromosome 3. J. Neuropathol. Exp. Neurol. *66*, 884–891.

Isaacs, A.M., Johannsen, P., Holm, I., and Nielsen, J.E. (2011). Frontotemporal dementia caused by CHMP2B mutations. Curr. Alzheimer Res. *8*, 246–251.

Jiang, Q., Lee, C.Y., Mandrekar, S., Wilkinson, B., Cramer, P., Zelcer, N., Mann, K., Lamb, B., Willson, T.M., Collins, J.L., et al. (2008).

ApoE promotes the proteolytic degradation of Abeta. Neuron *58*, 681–693.

Laskowitz, D.T., Thekdi, A.D., Thekdi, S.D., Han, S.K., Myers, J.K., Pizzo, S.V., and Bennett, E.R. (2001). Downregulation of microglial activation by apolipoprotein E and apoE-mimetic peptides. Exp. Neurol. *167*, 74–85.

Maki, R.A., Tyurin, V.A., Lyon, R.C., Hamilton, R.L., DeKosky, S.T., Kagan, V.E., and Reynolds, W.F. (2009). Aberrant expression of myeloperoxidase in astrocytes promotes phospholipid oxidation and memory deficits in a mouse model of Alzheimer disease. J. Biol. Chem. *284*, 3158–3169.

Martinez, E., Navarro, A., Ordonez, C., Del Valle, E., and Tolivia, J. (2012). Amyloid-beta25-35 induces apolipoprotein D Synthesis and growth arrest in HT22 hippocampal cells. J. Alzheimers Dis. *30*, 233–244.

Mwanjewe, J., and Grover, A.K. (2004). Role of transient receptor potential canonical 6 (TRPC6) in non-transferrin-bound iron uptake in neuronal phenotype PC12 cells. Biochem. J. *378*, 975–982.

Nguyen, H.N., Byers, B., Cord, B., Shcheglovitov, A., Byrne, J., Gujar, P., Kee, K., Schule, B., Dolmetsch, R.E., Langston, W., et al. (2011). LRRK2 mutant iPSC-derived DA neurons demonstrate increased susceptibility to oxidative stress. Cell Stem Cell *8*, 267–280.

Nielsen, T.T., Mizielinska, S., Hasholt, L., Isaacs, A.M., and Nielsen, J.E. (2012). Reversal of pathology in CHMP2B-mediated frontotemporal dementia patient cells using RNA interference. J. Gene Med. *14*, 521–529.

Ran, F.A., Hsu, P.D., Wright, J., Agarwala, V., Scott, D.A., and Zhang, F. (2013). Genome engineering using the CRISPR-Cas9 system. Nat. Protoc. *8*, 2281–2308.

Rasmussen, M.A., Holst, B., Tumer, Z., Johnsen, M.G., Zhou, S.L., Stummann, T.C., Hyttel, P., and Clausen, C. (2014). Transient p53 suppression increases reprogramming of human fibroblasts without affecting apoptosis and DNA damage. Stem Cell Rep. *3*, 404–413.

Rawson, R.L., Yam, L., Weimer, R.M., Bend, E.G., Hartwieg, E., Horvitz, H.R., Clark, S.G., and Jorgensen, E.M. (2014). Axons degenerate in the absence of mitochondria in *C. elegans*. Curr. Biol. *24*, 760–765.

Rossor, M.N., Fox, N.C., Mummery, C.J., Schott, J.M., and Warren, J.D. (2010). The diagnosis of young-onset dementia. Lancet Neurol. *9*, 793–806.

Urwin, H., Authier, A., Nielsen, J.E., Metcalf, D., Powell, C., Froud, K., Malcolm, D.S., Holm, I., Johannsen, P., Brown, J., et al. (2010). Disruption of endocytic trafficking in frontotemporal dementia with CHMP2B mutations. Hum. Mol. Genet. *19*, 2228–2238.

Wang, X., Yan, M.H., Fujioka, H., Liu, J., Wilson-Delfosse, A., Chen, S.G., Perry, G., Casadesus, G., and Zhu, X. (2012). LRRK2 regulates mitochondrial dynamics and function through direct interaction with DLP1. Hum. Mol. Genet. *21*, 1931–1944.

Xie, Y., Zhou, B., Lin, M.Y., Wang, S., Foust, K.D., and Sheng, Z.H. (2015). Endolysosomal deficits augment mitochondria pathology in spinal motor neurons of asymptomatic fALS mice. Neuron *87*, 355–370.